Published Online: 5 October, 2015 | Supp Info: http://doi.org/10.1083/jcb.201504097

Growth factor signaling to mTORC1 by amino acid–laden macropinosomes

Sei Yoshida,[1] Regina Pacitto,[1] Yao Yao,[2,3] Ken Inoki,[2,3] and Joel A. Swanson[1]

[1]Department of Microbiology and Immunology and [2]Department of Molecular and Integrative Physiology, University of Michigan Medical School, Ann Arbor, MI 48109
[3]Life Sciences Institute, University of Michigan, Ann Arbor, MI 48109

The rapid activation of the mechanistic target of rapamycin complex-1 (mTORC1) by growth factors is increased by extracellular amino acids through yet-undefined mechanisms of amino acid transfer into endolysosomes. Because the endocytic process of macropinocytosis concentrates extracellular solutes into endolysosomes and is increased in cells stimulated by growth factors or tumor-promoting phorbol esters, we analyzed its role in amino acid–dependent activation of mTORC1. Here, we show that growth factor-dependent activation of mTORC1 by amino acids, but not glucose, requires macropinocytosis. In murine bone marrow–derived macrophages and murine embryonic fibroblasts stimulated with their cognate growth factors or with phorbol myristate acetate, activation of mTORC1 required an Akt-independent vesicular pathway of amino acid delivery into endolysosomes, mediated by the actin cytoskeleton. Macropinocytosis delivered small, fluorescent fluid-phase solutes into endolysosomes sufficiently fast to explain growth factor–mediated signaling by amino acids. Therefore, the amino acid–laden macropinosome is an essential and discrete unit of growth factor receptor signaling to mTORC1.

Introduction

Macropinocytosis has long been associated with cell growth. Growth factors and tumor-promoting phorbol esters stimulate macropinocytosis in many metazoan cells (Swanson and Watts, 1995). Cells transformed by oncogenic Ras or v-Src exhibit increased macropinocytosis (Bar-Sagi and Feramisco, 1986; Swanson and Watts, 1995; Veithen et al., 1996). Proteins internalized and degraded through macropinocytosis support the growth of Ras-transformed cells (Commisso et al., 2013; Palm et al., 2015). Many intracellular signaling molecules implicated in cellular growth control, including phosphatidylinositol 3-kinase (PI3K) and Ras, are required for macropinosome formation and are active on macropinosomes (Porat-Shliom et al., 2008; Swanson, 2008; Mercer et al., 2010). Growth factor signaling cascades occur in subdomains of plasma membrane enclosed by circular ruffles of plasma membrane that close to form macropinosomes (Yoshida et al., 2009, 2015; Welliver and Swanson, 2012), which suggests that the forming macropinosome serves as a platform for signal transduction leading to growth.

Cell growth is regulated by mechanistic target of rapamycin complex-1 (mTORC1), a complex of cytosolic proteins that is activated by growth factor receptor signaling, tumor-promoting phorbol esters, and increased levels of amino acids inside endolysosomes (Roux et al., 2004; Efeyan et al., 2012). Amino acid–dependent signaling from growth factor receptors to mTORC1 requires activation of Rheb and Rag GTPases, which are themselves activated by two signaling pathways: (1) PI3K-dependent activation of Akt leads to phosphorylation and inhibition of TSC1/TSC2, which relieves inhibition of Rheb on endolysosomes (Menon et al., 2014); and (2) amino acids in endolysosomes are sensed by Ragulator on endolysosomal membranes, which in turn activates Rag GTPases (Jewell et al., 2013; Bar-Peled and Sabatini, 2014). Active mTORC1 regulates cellular metabolism, stimulating protein synthesis by phosphorylation of S6 kinase (S6K) and 4EBP1. How amino acids reach endolysosomes so quickly in response to growth factor signaling is not known. However, endolysosomes and endocytic trafficking contribute to the activation of mTORC1 by amino acids (Flinn et al., 2010; Li et al., 2010; Bridges et al., 2012). Because macropinocytosis internalizes and concentrates relatively large volumes of extracellular solutes (Swanson, 1989; Swanson and Watts, 1995), we tested the hypothesis that the macropinosome participates directly in growth factor receptor signal transduction through rapid internalization and delivery of amino acids into endolysosomes, where they activate mTORC1. Using mu-

Correspondence to Joel Swanson: jswan@umich.edu

Abbreviations used in this paper: BMM, bone marrow–derived macrophage; DPBS, Dulbecco's phosphate-buffered saline; EIPA, 5-(*N*-ethyl-*N*-isopropyl) amiloride; FDx70, fluorescein isothiocyanate-dextran molecular weight 70,000; gRNA, guide RNA; JB, jasplakinolide and blebbistatin; LY, Lucifer yellow; M-CSF, macrophage colony-stimulating factor; MEF, mouse embryonic fibroblast; MEK/ERK, MAP kinase/ERK kinase (MEK) and extracellular signal–related kinase (ERK); PI3K, phosphatidylinositol 3-kinase; PIP_3, phosphatidylinositol (3,4,5)-trisphosphate; RB, Ringer's buffer; S6K, S6 kinase; TRDx, Texas red–labeled dextran; WT, wild type.

The Rockefeller University Press $30.00
J. Cell Biol. Vol. 211 No. 1 159–172
www.jcb.org/cgi/doi/10.1083/jcb.201504097

rine macrophages and embryonic fibroblasts stimulated with their cognate growth factors or with PMA, we determined that mTORC1 activation requires the formation of amino acid–containing macropinosomes and subsequent fusion of those macropinosomes with endolysosomes.

Results

Macropinocytosis is required for macrophage colony-stimulating factor–induced amino acid–dependent mTORC1 activation in macrophages

mTORC1 and related biochemical signaling activities were characterized in bone marrow–derived macrophages (BMMs), which elicit robust macropinocytic responses to macrophage colony-stimulating factor (M-CSF) and PMA (Racoosin and Swanson, 1989; Swanson, 1989). mTORC1 activity, as measured by phosphorylation of S6K, increased within 5 min of adding M-CSF (Fig. 1 A). M-CSF also transiently increased the activities of MAP kinase/ERK kinase (MEK) and extracellular signal–related kinase (ERK) (MEK/ERK), PI3K, and mTORC2, another mTOR complex (Loewith et al., 2002; Shaw and Cantley, 2006). PMA increased the activity of mTORC1 and MEK, although more slowly than M-CSF, and did not stimulate PI3K or mTORC2 (Fig. 1 B). Amino acid–rich medium significantly increased mTORC1 activity in response to either M-CSF (Fig. 1 C) or PMA (Fig. 1 D), as did the inclusion of leucine in PBS (Fig. 1, E and F). Phosphorylation of 4EBP1, another indicator of mTORC1 activity, was also increased by leucine in cells stimulated with M-CSF or PMA (Fig. 1, E and F), although the effects were less pronounced, perhaps because of amino acid–independent phosphorylation of 4EBP1 by ERK (Blagden and Willis, 2011). Thus, M-CSF and PMA stimulated leucine-dependent activation of mTORC1 with different kinetics.

The delayed activation of mTORC1 by PMA relative to M-CSF was similar to the delay in stimulation of pinocytosis by these stimuli (Racoosin and Swanson, 1989). Quantitative microscopy of BMMs confirmed that M-CSF stimulated rapid increases in macropinosome formation, whereas PMA stimulated macropinosome formation more slowly (Fig. 2, A and B). Thus, the stimulation of macropinocytosis by M-CSF and PMA correlated with the timing of mTORC1 activation (Fig. 1, A and B).

PI3K is necessary for macropinosome formation (Araki et al., 1996) and stimulation of mTORC1 in response to growth factors (Zoncu et al., 2011b). PI3K stimulates mTORC1 by increasing Akt activity, which in turn phosphorylates TSC2 and relieves TSC1/TSC2 inhibition of the mTORC1-activating GTPase Rheb (Bar-Peled and Sabatini, 2014). We examined the relative contributions of type 1 PI3K isoforms to macropinocytosis and mTORC1 activation in BMMs in response to M-CSF and PMA. A66, an inhibitor of p110α of PI3K type 1a (Jamieson et al., 2011), partially inhibited phosphorylation of Akt and activation of mTORC1 by M-CSF, albeit at concentrations that were greater than those required to inhibit p110α (Fig. 2 C and Fig. S1 A). The p110δ-specific inhibitor IC87114 inhibited more effectively Akt phosphorylation (Fig. S1 B), macropinocytosis, and mTORC1 in response to M-CSF, and combined treatment with A66 and IC87114 inhibited these activities completely (Fig. 2 D and Fig. S1 B). Strikingly, neither inhibitor reduced macropinocytosis, mTORC1 activity or the phosphorylation of TSC2 in response to PMA (Fig. 2, E and F; and Fig. S1 C), suggesting that PMA stimulates macropinocytosis downstream of PI3K. Thus, stimulation of both macropinocytosis and mTORC1 was PI3K dependent for M-CSF and PI3K independent for PMA. Inhibition of MEK with U0126 (Favata et al., 1998) did not reduce activation of mTORC1 by M-CSF or PMA, indicating that mTORC1 activation in BMMs was independent of MEK/ERK signaling (Fig. S1, D and E). MK2206, a specific inhibitor of Akt (Hirai et al., 2010), which does not inhibit M-CSF–induced macropinocytosis in BMMs (Yoshida et al., 2015), inhibited M-CSF–induced phosphorylation of S6K and Akt (Thr308; Fig. S1 F), which suggests

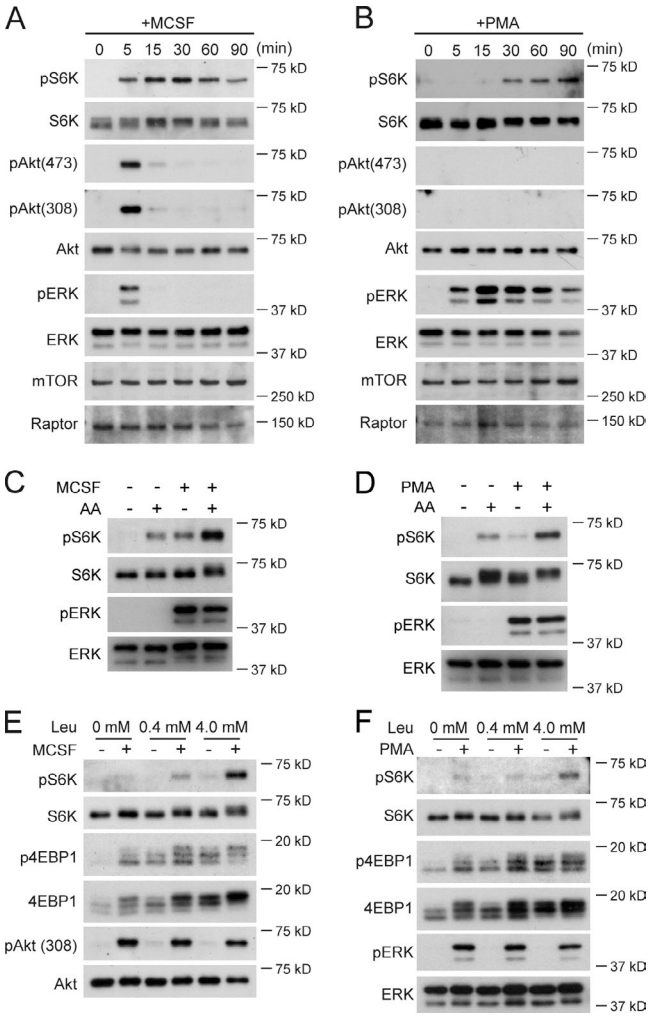

Figure 1. **Amino acids increase activation of mTORC1 by M-CSF and PMA in macrophages.** (A) Time course of signaling in BMMs after stimulation with M-CSF. mTORC1 activity, as indicated by phosphorylation of S6K (pS6K), increased within 5 min and remained elevated. PI3K (pAkt-308), mTORC2 (pAkt-473), and MEK/ERK (pERK) were activated transiently. (B) Time course of signaling in response to PMA. MEK/ERK activity increased quickly, whereas mTORC1 was activated after a delay. PI3K and mTORC2 were not activated. (C and D) Relative to amino acid–depleted medium (HBSS, –), amino acid–rich medium (DMEM, +) increased mTORC1 activation in response to M-CSF (5-min stimulation; C) and PMA (30-min stimulation; D), but did not affect stimulation of MEK/ERK in response to either stimulus. (E and F) The addition of leucine to DPBS was sufficient to augment activation of mTORC1 by M-CSF (E) or PMA (F), as indicated by phosphorylation of S6K and 4EBP1, but did not alter stimulation of PI3K by M-CSF or of MEK/ERK by PMA.

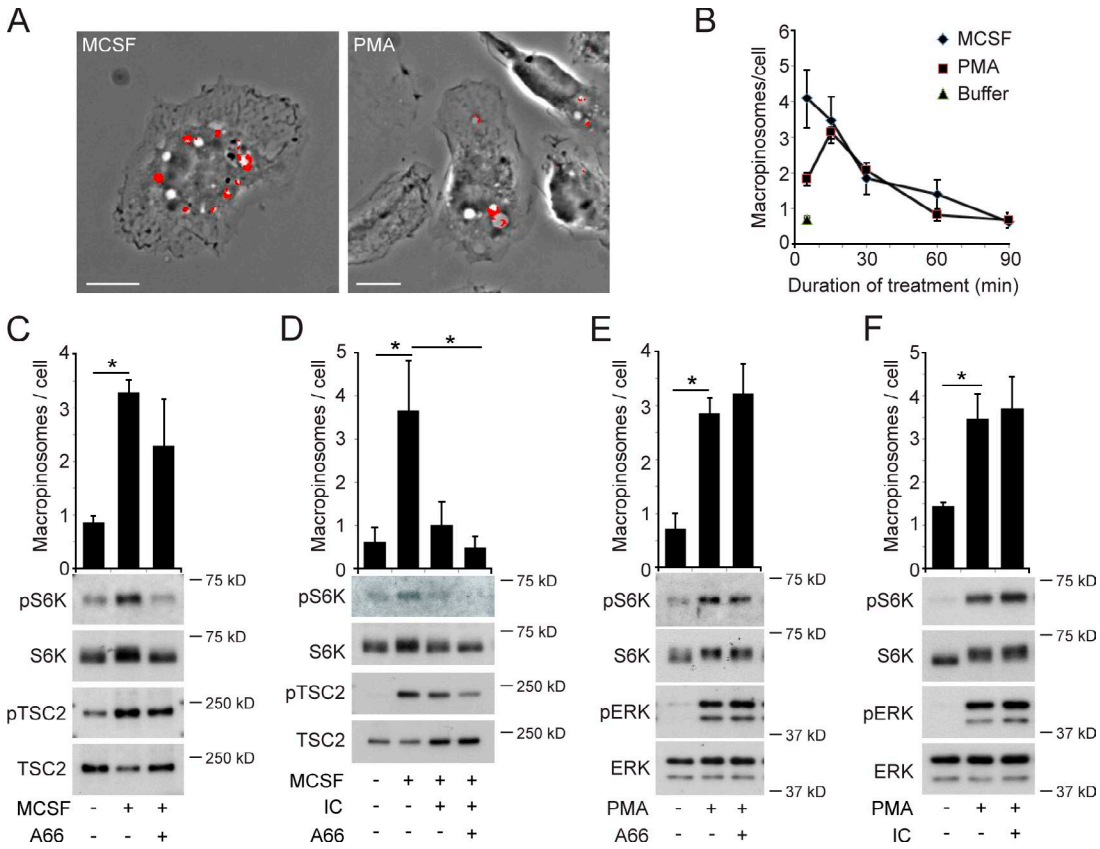

Figure 2. **Macropinocytosis is required for activation of mTORC1 by M-CSF and PMA in macrophages.** (A) Macropinosome formation in response to M-CSF and PMA. BMMs were incubated for 5 min in buffer containing fluorescein dextran with M-CSF or PMA, and then were washed, fixed, and observed by phase-contrast and fluorescence microscopy (red overlay; Bars, 10 µm). (B) Time course of macropinosome formation after stimulation with M-CSF (diamonds), PMA (squares), or with buffer only (triangle). $n \geq 25$ cells per time point. (C–F) Effects of PI3K inhibitors on macropinocytosis (top) and mTORC1 activity (bottom). M-CSF–stimulated macropinocytosis and mTORC1 activity were inhibited partially by A66 (C) and were inhibited more completely by IC87114 (IC) or the combination of IC87114 and A66 (D). PMA-stimulated macropinocytosis and mTORC1 activity were unaltered by either A66 (E) or IC (F). B–F show the means ± SEM from three independent experiments, with >25 cells scored per condition. *, $P < 0.05$, one-tailed *t* test.

that macropinocytosis required for the M-CSF–dependent mTORC1 activation is PI3K dependent but Akt independent.

Macropinocytosis requires actin-based motility. To test the effects of cytoskeletal inhibitors on macropinocytosis and mTORC1 activity, BMMs were pretreated with jasplakinolide and blebbistatin (JB), which inhibit actin depolymerization (Bubb et al., 1994) and myosin II (Straight et al., 2003), respectively. JB completely inhibited both macropinocytosis and the activation of mTORC1, without altering TSC2 phosphorylation in response to M-CSF or PMA (Fig. 3, A and B). JB also inhibited PMA-stimulated phosphorylation of 4EBP1 (Fig. 3 E). Moreover, the macropinocytosis-dependent activation of mTORC1 was specific for amino acids: leucine-dependent activation of mTORC1 was inhibited by JB (Fig. 3 C) but glucose-dependent activation was inhibited only slightly (Fig. 3 D). The macropinocytosis inhibitor 5-(*N*-ethyl-*N*-isopropyl) amiloride (EIPA; Koivusalo et al., 2010) also inhibited mTORC1 activation by M-CSF and PMA (Fig. 3, F and G). The effects of U0126 and EIPA on macropinocytosis in response to M-CSF correlated with their effects on mTORC1 activation (Fig. 3 H). Overall, the induction of macropinocytosis and mTORC1 by M-CSF and PMA showed corresponding patterns of sensitivity to inhibitors of macropinocytosis, PI3K, and MEK/ERK.

Macropinocytosis is required for PDGF-induced leucine-dependent mTORC1 activation in mouse embryonic fibroblasts

A role for macropinocytosis in amino acid–dependent stimulation of mTORC1 was also evident in mouse embryonic fibroblasts (MEFs) stimulated with PDGF. The addition of PDGF to serum-starved MEFs stimulated macropinocytosis (Fig. S2 A). Leucine increased activation of mTORC1 by PDGF without further increasing macropinocytosis (Fig. 4 A) and increasing concentrations of leucine yielded corresponding increases in mTORC1 activity (Fig. 4 B). As in BMMs, inhibition of macropinocytosis by EIPA or JB inhibited leucine-dependent activation of mTORC1 (Fig. 4, C and D) but did not inhibit glucose-dependent activation of mTORC1 (Fig. 4 E). The small GTPase Rac regulates actin polymerization and macropinocytosis (Ridley et al., 1992; Fujii et al., 2013). To examine the contribution of Rac1 to activation of mTORC1 by PDGF, we used CRISPR/Cas9 methods to prepare MEFs deficient in Rac1. Rac1 deficiency was confirmed by Western immunoblotting of lysates (Fig. S3 A). Stimulation of serum-starved Rac1-deficient MEFs with PDGF in DMEM or Dulbecco's phosphate-buffered saline (DPBS)/leucine resulted in significantly reduced dorsal ruffling and macropinosome formation, relative to control cells (Fig. S3, B–E). Likewise, activation of mTORC1 by PDGF was

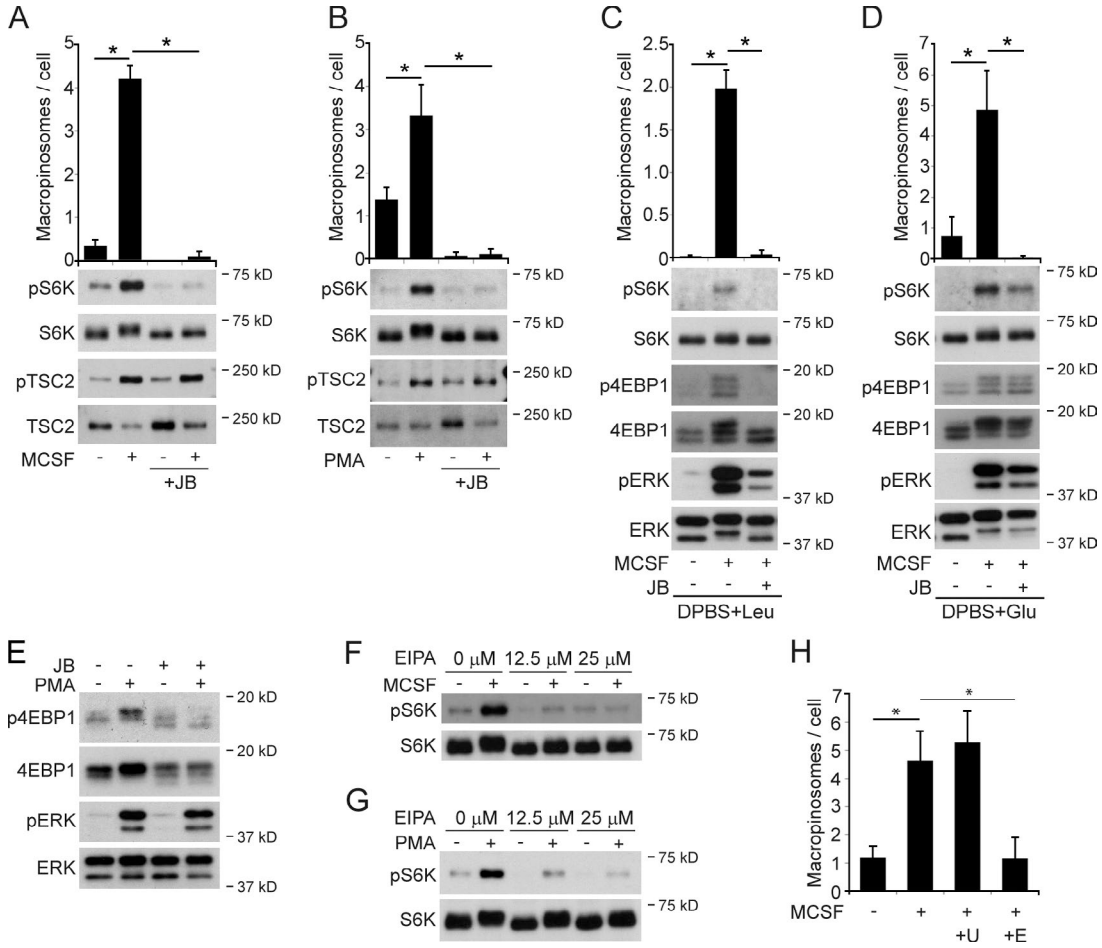

Figure 3. **Macropinocytosis is required for activation of mTORC1 in BMM.** (A–D) Effects of JB on macropinocytosis (top) and mTORC1 activity (bottom). JB treatment blocked both macropinocytosis and mTORC1 activity in response to M-CSF in DMEM (A), PMA in DMEM (B), or M-CSF in DPBS containing 0.4 mM leucine (C). (D) JB did not inhibit activation of mTORC1 in response to M-CSF in DPBS containing 5.6 mM glucose. (E) JB inhibited 4EBP1 phosphorylation in response to PMA in BMM. (F and G) EIPA inhibited activation of mTORC1 by M-CSF (5-min stimulation; F) and PMA (30-min stimulation; G). (H) Macropinosome formation in response to M-CSF was inhibited by EIPA (+E), but not by U0126 (+U). Macropinocytosis measurements of A–D and H show the means ± SEM from three independent experiments, with >25 cells scored per condition. *, $P < 0.05$, one-tailed *t* test.

reduced (Fig. S3 A). Together, these results support a role for actin-dependent macropinosome formation in the amino acid–dependent activation of mTORC1 by PDGF.

To address the possibility that leucine reached endolysosomes by leucine-specific transport across plasma membrane and endolysosomal membranes instead of endocytosis, we measured PDGF-dependent activation of mTORC1 in the presence of the dipeptide Ala-Leu, which should not readily cross membranes via amino acid transport proteins and must be hydrolyzed to amino acids to activate mTORC1. After a delay of 30 min, extracellular Ala-Leu increased PDGF-dependent phosphorylation of S6K (Fig. 4 F), indicating that stimulation of mTORC1 in MEFs by PDGF requires the endocytosis of Ala-Leu into macropinosomes and subsequent degradation to alanine and leucine.

Previous studies established that PDGF stimulates amino acid–dependent phosphorylation of S6K in MEFs, in part because of PI3K-dependent phosphorylation of TSC2 by Akt (Bar-Peled and Sabatini, 2014). Because JB caused a slight inhibition of TSC2 phosphorylation (Fig. 4 D), we examined the roles of Akt and TSC2 in macropinocytosis-dependent activation of mTORC1 by PDGF. As in BMMs (Fig. S1 F; Yoshida et al., 2015), the Akt inhibitor MK2206 inhibited phosphorylation of S6K and Akt (Thr308) completely without inhibiting macropinocytosis (Fig. 4 G), indicating that Akt was necessary for activation of mTORC1 and independent of macropinocytosis. To examine the role of macropinocytosis relative to Akt/TSC2/Rheb, mTORC1 activity was measured in wild-type (WT) and TSC2-deficient MEFs after stimulation with PDGF in the presence or absence of JB. S6K phosphorylation was elevated in TSC2-deficient MEFs, relative to WT MEFs, but could be further increased by PDGF (Fig. 4 H). Moreover, the PDGF-dependent increase in mTORC1 and macropinocytosis could be inhibited by JB (Fig. 4 H and Fig. S2, B and C). PLCγ1-DAG-PKC pathways activated by M-CSF in BMMs are necessary for macropinocytosis and are independent of Akt activation (Yoshida et al., 2015). Similarly, the PDGF-stimulated increase in macropinocytosis and mTORC1 activity in both WT and TSC2-deficient MEFs could be inhibited by the PKC inhibitor calphostin C (Fig. 5). Collectively, these results indicate that two independent pathways downstream of PI3K (Akt/TSC1/TSC2/Rheb and PKC-dependent macropinocytosis) are each necessary but not sufficient for amino acid–dependent activation of mTORC1 by growth factors.

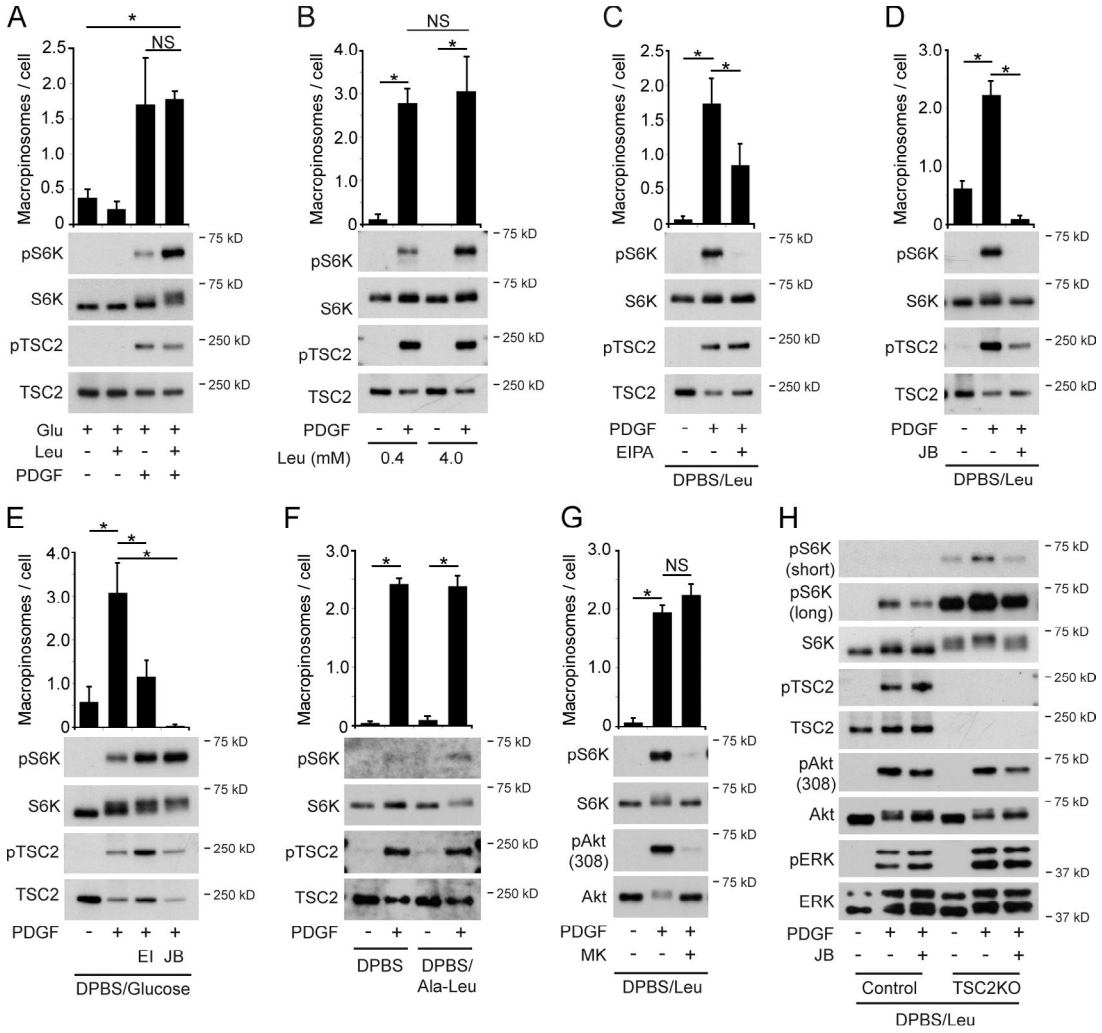

Figure 4. **Macropinocytosis is required for leucine-dependent activation of mTORC1 by PDGF in MEFs.** (A) Amino acid–dependent activation of mTORC1 by PDGF. MEFs were incubated 30 min in DPBS and then stimulated for 15 min with PDGF (2 nM) in DPBS containing glucose (Glu; 5.6 mM) and leucine (Leu; 0.4 mM) and scored for macropinosome formation (top) and mTORC1 activity (bottom). (B) Effects of leucine concentration on macropinocytosis (top) and mTORC1 activity (bottom). (C and D) Stimulation of macropinocytosis and mTORC1 by PDGF and 0.4 mM leucine were inhibited by EIPA (C) and JB (D). (E) Stimulation of mTORC1 by PDGF and glucose (5.6 mM) was not inhibited by EIPA (EI) or JB. (F) Activation of mTORC1 after 30 min in PDGF and Ala-Leu. MEFs were incubated in DPBS for 30 min, followed by 30 min in DPBS, with or without PDGF, with or without 4 mM Ala-Leu. (G) Effects of Akt inhibitor MK2206 (MK; 2 µM for 30 min) on macropinocytosis (top), Akt activity, and mTORC1 (bottom). Macropinocytosis measurements of A–G show the means ± SEM from three independent experiments, with >25 cells scored per condition. *, $P < 0.05$, one-tailed *t* test. (H) Stimulation of mTORC1 in TSC2-deficient (TSC2KO) and WT MEFs. mTORC1 activity in TSC2KO MEFs was increased by PDGF and inhibited by JB.

Growth factors increase amino acid–dependent recruitment of mTOR to macropinosomes and endolysosomes

Amino acids stimulate Rag GTPases, which recruit mTORC1 to endolysosomes, where mTORC1 is directly activated by Rheb (Sancak et al., 2008; Zoncu et al., 2011a). If macropinocytosis is essential for rapid amino acid–dependent activation of mTORC1, then macropinosomes formed in response to growth factors should deliver extracellular amino acids to endolysosomes within a few minutes of stimulation or serve as mTORC1 signaling platforms themselves. To test this, we examined mTOR localization in BMMs and whether extracellular fluid-phase solutes reach endolysosomal compartments via macropinocytosis on a time scale comparable to mTORC1 activation. BMMs were stimulated for 5 min in medium containing M-CSF and were then fixed and stained for immunofluorescence localization of LAMP-1, which localizes to endolysosomes and some macropinosomes (Racoosin and Swanson, 1993; Huotari and Helenius, 2011), mTOR, and RagC, which localizes to lysosomes and binds to activated mTORC1. In BMMs, endolysosomes often take the form of tubulovesicular networks (Knapp and Swanson, 1990). Immunofluorescence of BMMs fixed 5 min after addition of M-CSF showed colocalization of LAMP-1–positive macropinosomes and tubular endolysosomes with mTOR (Fig. 6, A and B and Fig. S4 A) and with RagC (Fig. S4 B). The presence of amino acids increased the frequency of cells showing mTOR–LAMP-1 colocalization (Fig. S4 C), suggesting that, as in other cell types stimulated by growth factors, the movement of amino acids into BMM endolysosomes increased mTOR recruitment to endolysosomes. To infer endocytosis and accumulation of extracellular amino acids by BMMs, we monitored the endocytosis of the low molecular weight, fluorescent, fluid-phase probe Lucifer yellow (LY; Berthiaume et al., 1995). Incubation of BMMs for 1 or

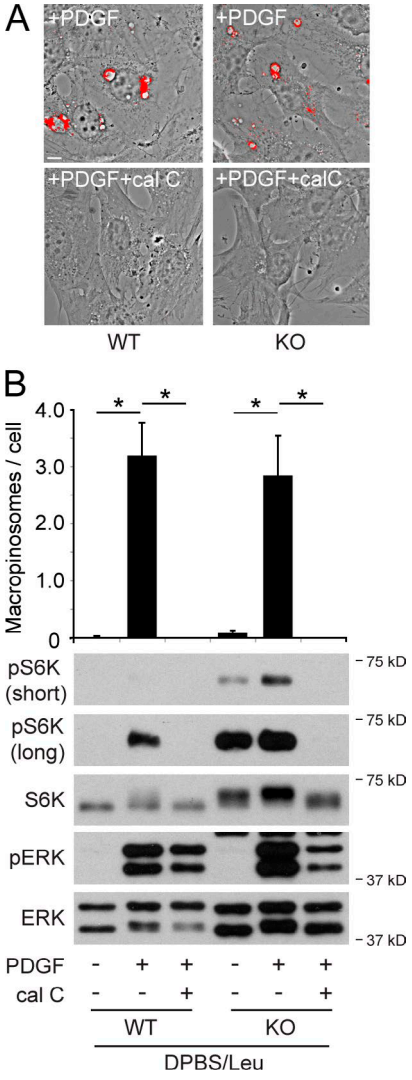

Figure 5. **PKC inhibition blocks PDGF-induced macropinocytosis and mTORC1 activation independent of TSC function.** (A) Macropinosome formation in TSC2-WT (left) and TSC2-knockout (KO) (right) MEFs stimulated by PDGF in the presence of FDx with (bottom) or without (top) calphostin C (cal C). FDx-labeled macropinosomes are indicated by red overlay. Bar, 10 µm. (B) Macropinocytosis and activation of mTORC1 in TSC2-WT and TSC2-KO MEFs was increased by PDGF and inhibited by calphostin C. Bars indicate the means ± SEM of three trials. *, $P < 0.05$.

5 min with M-CSF and LY, followed by fixation and imaging, revealed LY in macropinosomes (Fig. 6 C), which sometimes colocalized with LAMP-1 (Fig. 6 E). After 10-min incubation with LY and M-CSF, however, some LY localized to LAMP-1–positive tubular endolysosomes (Fig. 6, C and F). Quantitation of images showed that M-CSF significantly increased overall LY accumulation by BMMs (Fig. 6 D), as observed previously (Racoosin and Swanson, 1989). We then examined the redistributions of endocytosed LY relative to mTOR. Pulse labeling macropinosomes for 5 min with LY showed limited colocalization with mTOR (Fig. S4 D). Inclusion of leucine in DPBS did not increase the frequency of macropinosome formation in response to M-CSF (Fig. S4 F), but it increased the percentage of macropinosomes with associated mTOR (Fig. S4, D, E, and G). This indicates that nutrient-rich macropinosomes can recruit mTOR, most likely via increased association of endolysosomes with macropinosomes. After 10 min, LY and mTOR colocalized on tubular endolysosomes (Fig. 6 G), and M-CSF increased that colocalization to a small but significant extent (Fig. 6 H). To examine the contribution of macropinocytosis to LY/mTOR colocalization, we overexpressed inhibitory Rac1-N17 (Rac1-DN) or WT Rac1 from IRES2-mCFP vectors and measured macropinocytosis, LY accumulation, and mTOR/LY colocalization in CFP-positive BMM. Relative to cells overexpressing WT Rac1, cells expressing Rac1-DN inhibited macropinosome formation (Fig. 6 I), the increased LY accumulation induced by M-CSF (Fig. 6 J), and the increased colocalization of LY with mTOR (Fig. 6 K and Fig. S4 H). Finally, we examined the contribution of amino acids to LY/mTOR colocalization. Inclusion of amino acids in the medium did not alter the net accumulation of LY by BMMs (Fig. 6 L), but it significantly increased the colocalization of endocytosed LY with mTOR (Fig. 6 M and Fig. S4 I). Thus, M-CSF–induced macropinocytosis conveys extracellular amino acids to the tubular endolysosomes, where mTORC1 is recruited and activated.

mTOR redistribution was more pronounced in MEFs. Immunofluorescence of mTOR and LAMP-1 after a 10-min stimulation with amino acids showed that mTOR localized to LAMP-1–positive organelles (Fig. S5 A), as observed previously (Yoshida et al., 2011), and the extent of colocalization was increased by PDGF (Fig. S5, A and B). Simply including leucine in DPBS with PDGF was sufficient to increase colocalization (Fig. S5, C–E), and PDGF-induced colocalization of mTOR and LAMP-1 could be inhibited by JB (Fig. S5, F and G). These results indicate that the macropinosome delivers leucine quickly into endolysosomes and itself matures rapidly into a LAMP-1–positive platform for activation of mTORC1.

M-CSF–induced macropinosomes rapidly deliver extracellular small solutes into endolysosomes in macrophages

To determine the timing of macropinocytic delivery of extracellular solutes to endolysosomes, macropinosome dynamics were analyzed by live cell imaging. Macrophage endolysosomes were labeled by endocytosis of Texas red–labeled dextran (TRDx), and cells were then observed by time-lapse phase-contrast and fluorescence microscopy after the addition of M-CSF. Phase-contrast images showed ruffling and macropinosome formation in response to M-CSF, and TRDx fluorescence showed the relative distributions of tubular and vesicular endolysosomes (Fig. 7 A and Video 1). Endolysosomes surrounded macropinosomes soon after they closed into the cell, and then the organelles separated and reconnected repeatedly as the macropinosomes gradually shrank, interactions that were reminiscent of a phenomenon termed piranhalysis (Willingham and Yamada, 1978) or kiss and run (Desjardins, 1995). To image the movements of endocytosed solutes, BMMs with TRDx-labeled endolysosomes were pulse labeled for 3 min with LY during stimulation with M-CSF. Immediately after the pulse labeling, various sizes of LY-labeled macropinosomes could be observed among TRDx-labeled tubular and vesicular endolysosomes (Fig. 7 B, Video 2, and Video 3). Macropinosomes merged into the endolysosomal compartment during the first few minutes. Tubular endolysosomes often wrapped around larger, phase-bright macropinosomes in a process similar to that described previously for phagosome-lysosome fusion (Fig. 7 B, $t = 7{:}40$; Knapp and Swanson, 1990). Mixing of compartment contents was indicated by colocalization of the two dyes in the macropi-

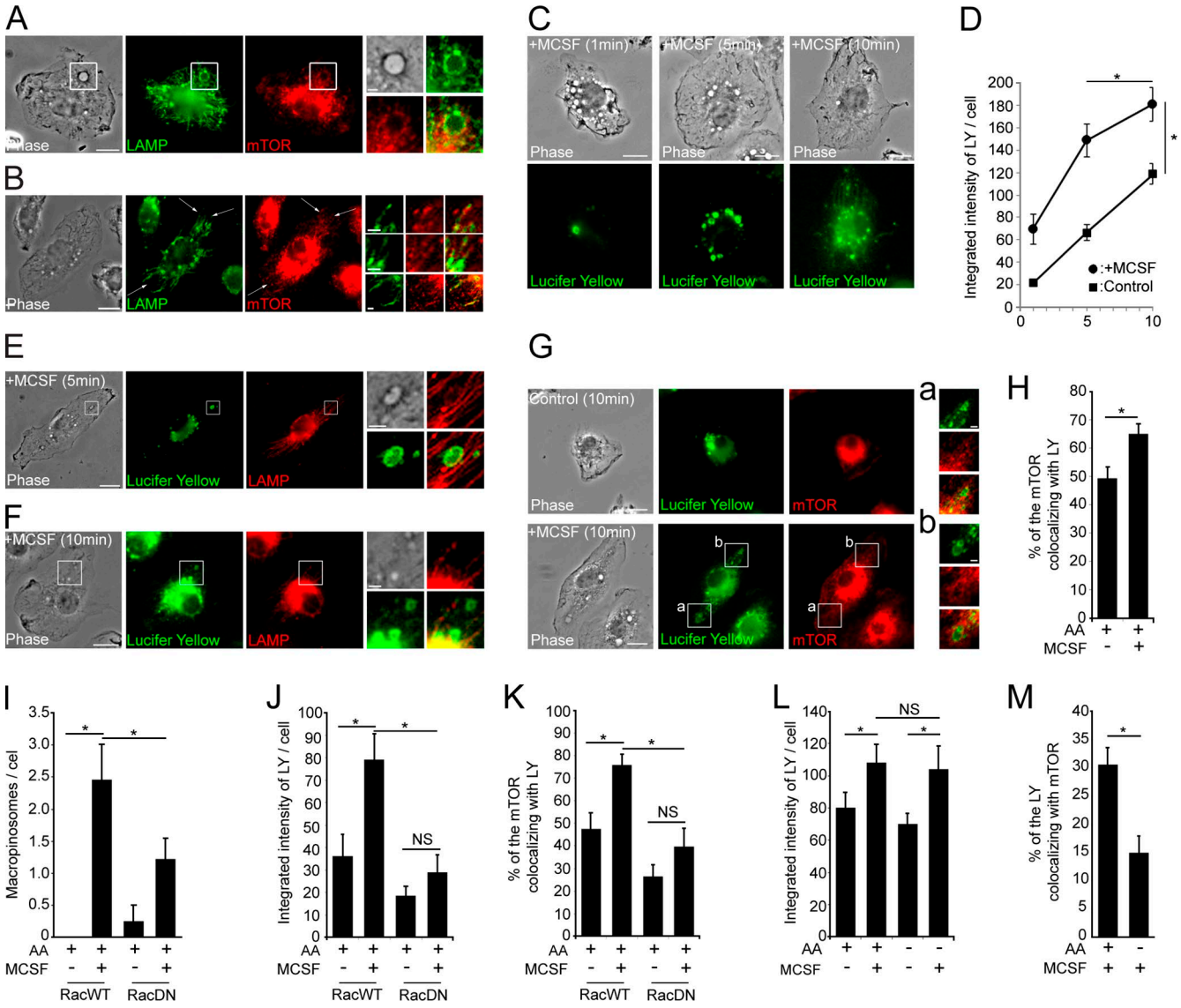

Figure 6. **Stimulation of macropinocytosis in BMMs increased solute uptake and amino acid–dependent recruitment of mTOR to macropinosomes and endolysosomes.** (A and B) Immunofluorescence localization of mTOR and LAMP-1 in BMMs stimulated 5 min with M-CSF. Insets show mTOR association with macropinosome-associated endolysosomes (A) and with tubular endolysosomes (B). (C) BMMs fixed and imaged after 1, 5, or 10 min with LY and M-CSF. LY was initially distributed in macropinosomes but also localized to tubular compartments by 10 min. (D) Total LY fluorescence per cell, from image analysis of preparations shown in C (n > 10 cells per point; *, $P < 0.05$). (E and F) Immunofluorescence localization of LAMP-1 after incubation of BMMs with LY and M-CSF for 5 min (E) or 10 min (F). Insets shows a macropinosome (E) and tubular endolysosomes (F) labeled with both LAMP-1 (top right) and LY (bottom left); top left: phase-contrast, bottom right: overlay. (G) Immunofluorescence localization of mTOR after 10-min incubation in LY with (bottom; insets a and b) or without (top) M-CSF. (H) Quantitation of mTOR colocalization with LY (*, $P < 0.05$). (I–K) Macropinocytosis and colocalization of mTOR and LY in BMMs expressing pRac1WT-IRES2-mCFP (RacWT) or pRac1(N17)-IRES2-mCFP (RacDN), fixed after stimulation for 5 min with FDx (I) or 10 min with LY (J and K) with or without M-CSF. CFP-positive BMMs were scored for macropinosome labeling with FDx (I), integrated intensity of LY per cell (J), and colocalization of mTOR with LY (K). RacDN significantly decreased macropinocytosis, LY accumulation, and mTOR colocalization with LY-positive organelles (*, $P < 0.05$). (L and M) Effects of amino acids on LY accumulation and colocalization of mTOR and LY. BMMs were incubated 10 min in DMEM (+AA) or HBSS (−AA) containing LY, with or without M-CSF. Amino acids did not affect the integrated cellular accumulation of LY (L), but increased the association of mTOR with LY-positive endocytic compartments (M). *, $P < 0.05$. Bars, 10 µm.

nosome (Fig. 7 B, t = 8:00), which then disappeared shortly afterward. The rapid shrinkage of macropinosomes after their luminal connection with the tubular endolysosomes (Fig. 7 B, Video 2, and Video 3) indicated that hydrostatic pressure in the endolysosomal compartment was negative relative to the macropinosomes, which could facilitate delivery of solutes into the endolysosomal compartment. On the basis of earlier studies showing that movement of fluid-phase solutes between endocytic compartments varies with molecular size (Berthiaume et al., 1995; Chen et al., 2015), we predicted that small solutes such as amino acids would exchange more quickly than larger solutes between macropinosomes and endolysosomes. To measure size-dependent exchange of solutes between compartments, macrophage endolysosomes were prelabeled by endocytosis of both TRDx (10-kD average mol wt) and the much smaller LY (457 g/mol). Cells were then stimulated with M-CSF and the delivery of fluorescent dyes into macropinosomes was measured by ratiometric fluorescence microscopy

(Fig. 7 C, Video 4, and Video 5). LY consistently transferred from endolysosomes to macropinosomes earlier than the larger TRDx, as indicated by transient increases of LY/TRDx fluorescence ratios in macropinosomes (Fig. 7 C, t = 26:20; and Video 4). Thus, small solutes internalized by macropinocytosis move quickly into and between endocytic compartments on a time scale consistent with M-CSF signaling to mTORC1.

Signaling for mTORC1 activation was localized to M-CSF–induced macropinocytic cups

The PI3K-independent stimulation of mTORC1 and macropinocytosis by PMA suggests that PMA, as a DAG analogue, functions downstream of PI3K in activating PKC necessary for macropinosome formation. Consistent with this hierarchy, localization of phosphatidylinositol (3,4,5)-trisphosphate (PIP_3) and DAG in BMMs stimulated with M-CSF indicated that the peak of PIP_3 generation in macropinocytic cups preceded the peak of DAG generation (Fig. 8, A and B; Yoshida et al., 2015). Moreover, PIP_3 did not appear in macropinosomes formed in response to PMA (Fig. 8 C). Thus, the pharmacological inhibitors and live cell imaging support a model in which growth factor signaling to macropinocytic cups initiates two PI3K-dependent pathways leading to mTORC1 activation and, further, that PMA signaling activates both pathways downstream of PI3K (Fig. 8, D and E).

Discussion

Macropinosome formation and subsequent delivery of fluid-phase solutes to endolysosomes provides a mechanism for rapid activation of mTORC1 by amino acids. Concentration of amino acids into endolysosomes by macropinocytosis is more efficient than by endocytosis of smaller vesicles, such as clathrin-coated vesicles, because macropinosomes internalize much greater volumes of extracellular fluid and retain a larger fraction of internalized solutes (Swanson, 1989). On the basis of this work, as well as earlier studies showing that PLCγ acts downstream of PI3K during macropinosome formation in v-Src–transformed fibroblasts (Amyere et al., 2000), we propose that normal growth factor receptor signaling to mTORC1 consists of a cytosolic pathway, composed of PI3K, Akt, TSC1/TSC2, and Rheb, and a vesicular pathway, which uses PI3K, PLCγ1, and PKC to create a novel unit of signal transduction, the amino acid–laden macropinosome (Fig. 8, D and E). Akt is not necessary for macropinosome formation (Fig. 4 G; Yoshida et al., 2015); however, activation of Akt and the cytosolic pathway may originate in the circular ruffles that become macropinosomes. Fluorescent PIP_3-binding proteins localize to circular ruffles in BMMs stimulated with M-CSF (Fig. 8 A; Yoshida et al., 2015). Signal amplification and propagation may be limited to those domains by barriers to lateral diffusion that are intrinsic to ruffle structure (Welliver et al., 2011; Welliver and Swanson, 2012).

Rac1 was implicated previously in the regulation of mTORC1 (Saci et al., 2011); Rac1 binds to mTOR independently of its GTP-binding status, and sequesters it in a regulatory manner. Our results indicate a role for Rac1 activity, specifically that related to actin-dependent macropinosome formation, in the activation of mTORC1 by M-CSF.

The role of Rab5 in activation of mTORC1 (Li et al., 2010; Bridges et al., 2012) may be explained by its effects on macropinosome formation and stability. Earlier studies established that macropinosomes are Rab5 positive before they fuse with endolysosomes (Porat-Shliom et al., 2008; Yoshida et al., 2009) and that Rab5 is active on macropinosomes and regulates macropinosome stability (Feliciano et al., 2011). The cycle of Rab5 activation and deactivation may therefore be necessary for macropinosome formation and the delivery of amino acids into endolysosomes.

These results are consistent with a role for PKC in macropinosome formation and mTORC1 activation, even in MEFs with constitutively active Rheb. The PI3K-independent activation of mTORC1 by PMA reported here indicates that phorbol esters stimulate both the cytosolic pathway, as reported previously (Tee et al., 2003; Roux et al., 2004), and a vesicular pathway, by triggering macropinosome formation downstream of PLCγ1.

Our studies demonstrate that macropinosomes elicited by growth factor stimulation deliver a bolus of amino acids to endolysosomes rapidly enough to activate mTORC1. Other types of endocytosis, such as clathrin-mediated endocytosis, which accumulate solutes in endolysosomes less efficiently than macropinocytosis, should also be capable of delivering amino acids to endolysosomes and activating mTORC1, independent of growth factor stimulation. For example, unstimulated macrophages accumulate as much LY in 60 min as macrophages stimulated for 10 min with M-CSF (Racoosin and Swanson, 1989). This suggests that macropinocytosis-independent activation of mTORC1 should become evident with longer incubations of starved cells with amino acids or with higher external concentrations of amino acids. Indeed, recent studies by Palm et al. (2015), which demonstrated a role for macropinocytosis-mediated protein accumulation in the activation of mTORC1, also showed that activation of mTORC1 by the addition of essential amino acids to amino acid–starved MEFs was independent of macropinocytosis. The apparent discrepancy between those results and the data reported here is likely attributable to the time scales used in the two studies. Unlike our analysis of rapid growth factor signaling (5–15 min), Palm et al. (2015) measured mTORC1 activity after 1–4 h in amino acid–replete medium. The longer incubations may have been sufficient to allow non-macropinocytotic endocytosis to supply enough amino acids to endolysosomes for activation of mTORC1.

In contrast with amino acids, signaling to mTORC1 by glucose was independent of macropinocytosis. This observation is consistent with an earlier study that implicated the membrane traffic protein Rab5 in the activation of mTORC1 by amino acids but not by glucose (Li et al., 2010). Recent studies have shown that stimulation of mTORC1 by leucine is different from the mechanisms of stimulation by arginine or glutamine, which use the transporter SLC38A9 (Rebsamen et al., 2015; Wang et al., 2015) and distinct vesicular pathways (Jewell et al., 2015).

These studies further suggest that macropinosomes are organizational units of growth factor receptor signaling. The uptake and concentration of amino acids and other solute nutrients into endolysosomes by macropinocytosis may be essential to growth factor receptor signaling at steady state. Although signaling is most often studied in the context of acute stimulation of cells after growth factor deprivation, the rapid stimulation of mTORC1 by amino acids in that setting may be an artifact of the experimental system. In the in vivo setting of constant concentrations of growth factor, receptor signaling may occur primarily through the stochastic, transient construction of macropinosomes. Accordingly, growth factor receptor signal cas-

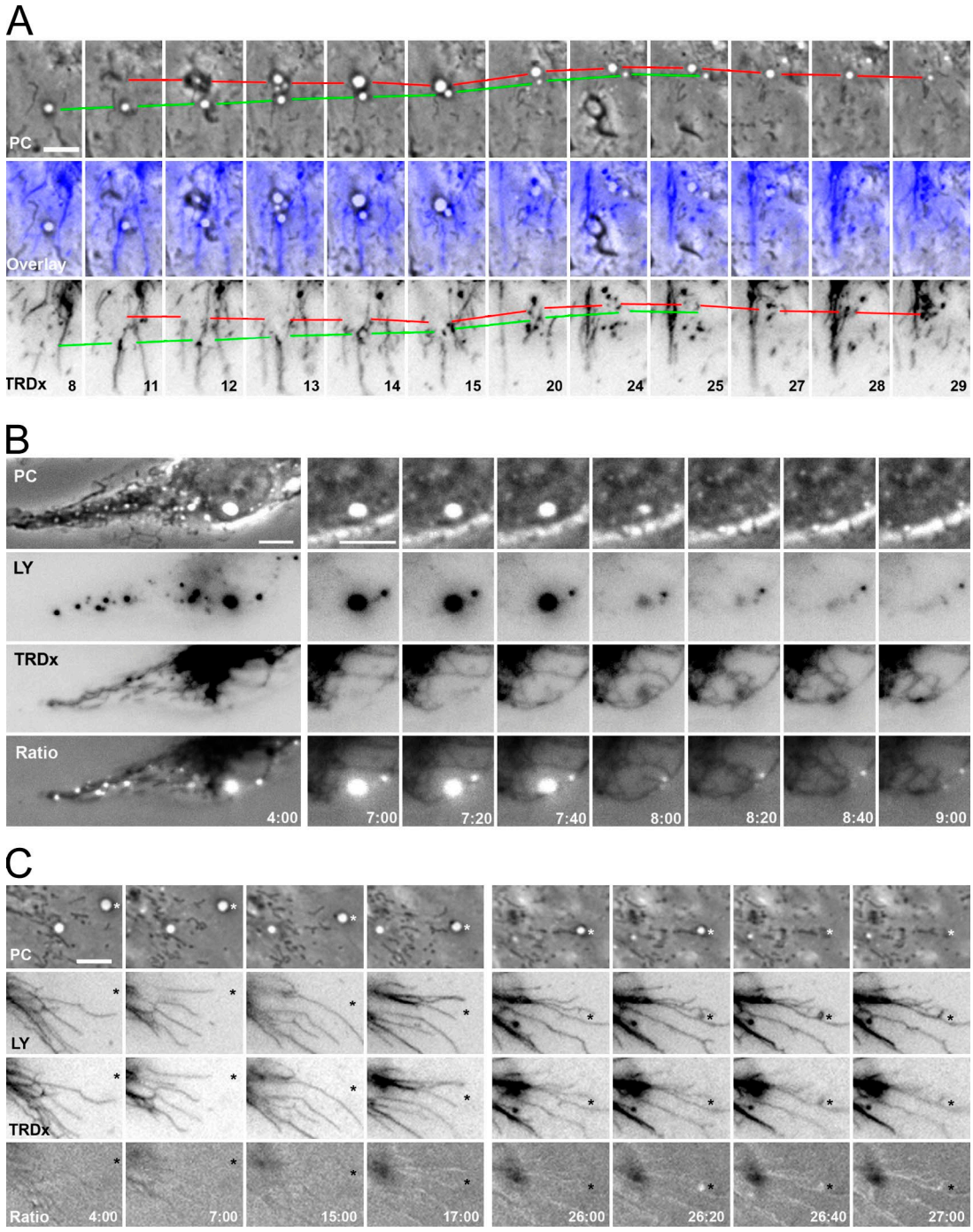

Figure 7. **Rapid delivery of extracellular small solutes into endolysosomes by M-CSF–induced macropinosomes in macrophages.** (A) BMMs with TRDx-labeled endolysosomes were stimulated with M-CSF and then imaged by time-lapse phase contrast (PC) and fluorescence (TRDx) microscopy. Corresponding distributions of macropinosomes and lysosomes are indicated in overlay images (middle row) and by the lines that track macropinosomes between time points (top and bottom rows). Time after the addition of M-CSF is indicated in the bottom row (minutes). Macropinosomes were repeatedly engaged by endolysosomes and shrank gradually. (B) PC images show phase-bright macropinosomes and the time course of maturation for one LY-labeled macropinosome. Inverted contrast images of macropinosomes (LY) and endolysosomes (TRDx) show dye exchange between the compartments. Time after addition of M-CSF is indicated in the bottom row (min:sec). LY/TRDx fluorescence ratio images (Ratio) show the relative distributions of macropinosomes (white) and endolysosomes (black). Tubular endolysosomes containing TRDx elongated toward the phase-bright macropinosome containing LY (t = 7:00–7:20), and wrapped around it (t = 7:40). The two dyes mixed in the macropinosome (t = 8:00), which then disappeared quickly (t = 8:00–9:00). (C) Size-selective solute exchange between tubular endolysosomes and macropinosomes. Tubular endolysosomes prelabeled with LY and TRDx contacted phase-bright macropinosomes and delivered LY before delivery of the larger TRDx. Asterisks indicate the position of a macropinosome in corresponding PC, LY, and TRDx fluorescence images. LY/TRDx ratio images show the early entry of LY into the macropinosome (26:20), followed by entry of the TRDx and rapid shrinkage of the macropinosome (26:40). Bars, 5 µm.

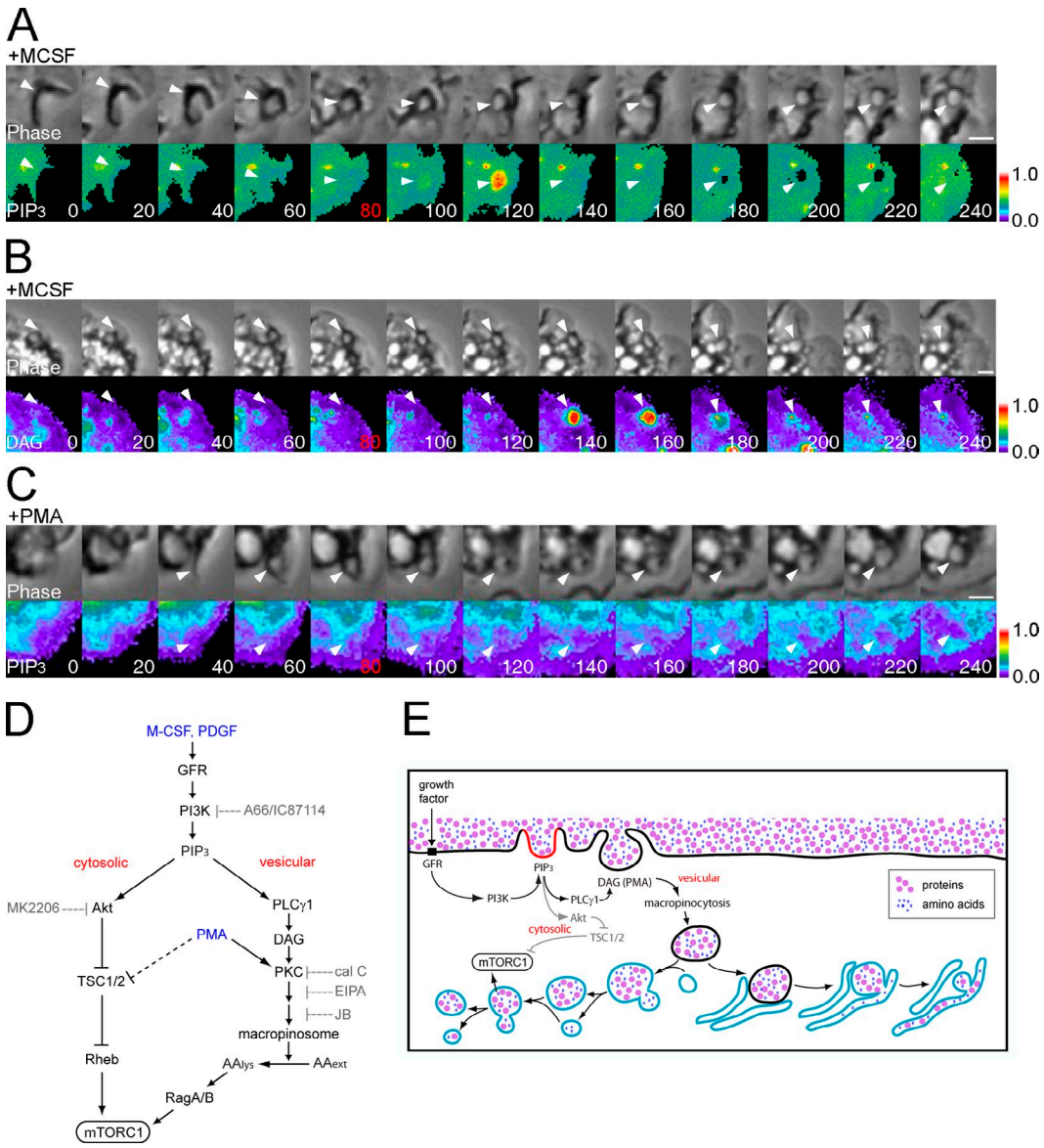

Figure 8. **Signaling for mTORC1 activation is localized to macropinocytic cups.** (A) BMMs expressing CFP and YFP-BtkPH, a probe for PIP_3, were imaged during M-CSF–stimulated macropinocytosis. The image series are aligned such that circular ruffle closure occurs at t = 80 s (top row). Pseudocolor ratio images (YFP-BtkPH/CFP) show strong YFP-BtkPH recruitment to the macropinocytic cup at t = 120 s (bottom row). (B) Ratiometric imaging of the DAG probe C1δ-YFP in BMMs, as described in (A). t = 80 s marks the end of ruffle closure. Maximal C1δ-YFP recruitment occurs at t = 140 and 160 s (C) Ratiometric imaging of the PIP_3 probe YFP-BtkPH during PMA-stimulated macropinocytosis. YFP-BtkPH was not recruited to the macropinocytic cup. Bars, 5 µm. (D) Two pathways of growth factor receptor (GFR) signaling to mTORC1. GFR signaling activates PI3K, which activates mTORC1 by a cytosolic pathway, involving Akt, TSC2, and Rheb, and a vesicular pathway, involving PKC-dependent, macropinosome-mediated delivery of leucine to endolysosomes. PMA activates both pathways independent of PI3K. Stimuli are indicated in blue type; inhibitors are indicated in gray type. (E) The macropinosome as a discrete unit of GFR signaling. PI3K-generated PIP_3 accumulates in macropinocytic cups (red line), activating Akt (cytosolic pathway) and PLCγ. PLCγ generates DAG in the cup, leading to PKC-dependent macropinocytosis (vesicular pathway). Extracellular solutes internalized by macropinocytosis are delivered rapidly into LAMP-1 (blue lines)–enriched endolysosomes by piranhalysis or after tubular endolysosomes wrap around macropinosomes. Small solutes exchange more rapidly between macropinosomes and endolysosomes than large solutes, providing a rapid mechanism for activation of mTORC1 by amino acids inside macropinosomes and endolysosomes.

cades occur within macropinocytic cups (Yoshida et al., 2009; Welliver and Swanson, 2012) and growth signals are propagated by delivering a bolus of amino acids into endolysosomes, or a bolus of proteins that are later hydrolyzed to amino acids in endolysosomes, thereby activating mTORC1. Moreover, the regulation of solute accumulation by macropinocytosis, positively by growth factors or negatively by feedback inhibition through mTORC1 (Palm et al., 2015) would modulate the flux of extracellular nutrients into the endolysosomal compartment and, consequently, the level of stimulus for cell growth. In transformed cells that form macropinosomes continuously, the unrestrained delivery of amino acids into endolysosomes may force mTORC1 activation and continued cell growth.

Materials and methods

Materials

M-CSF was from R&D Systems. PMA, U0126, LY294002, and leucine were from Sigma-Aldrich. EIPA, fluorescein isothiocyanate-dextran

molecular weight 70,000 (FDx70), TRDx (molecular weight 10,000), and LY were from Life Technologies. Blebbistatin and mouse PDGF BB were from Abcam. Jasplakinolide was from Enzo Life Sciences. A66 and IC87114 were from Symansis. MK2206 was from Apex-Bio. Calphostin C was from Calbiochem. DPBS, calcium (+), and magnesium (+) were from Life Technologies (14040). Alanyl dipeptide, Ala-Leu, was from Sigma-Aldrich. Anti–LAMP antibody (1D4B) was from the Developmental Studies Hybridoma Bank (Chen et al., 1985). Anti–mTOR (2983), anti–raptor (2280), anti–RagC (3360), anti–S6K (2708), anti–phospho-S6K (Thr389; 9234), anti–Akt (9272), anti–phospho-Akt (Thr308; 4056), anti–phospho-Akt (Ser473; 4060), anti–Erk1/2 (4695), anti–phospho-Erk1/2 (Thr202/Tyr204; 4376), anti–4EBP1 (9644), anti–phospho-4EBP1 (Thr37/46; 2855), anti–TSC2 (4308), and anti–phospho-TSC2 (Thr1462; 3617) antibodies were from Cell Signaling (Inoki et al., 2002; Sancak et al., 2008; Yoshida et al., 2011; Zoncu et al., 2011a). Anti–Rac1 (mouse) and anti–α-tubulin (mouse) were from Abcam. HRP-conjugated goat anti–rabbit IgG was from GE Healthcare. Texas red goat anti–rat IgG, Alexa Fluor 594 goat anti–rat IgG, Alexa Fluor 488 goat anti–rabbit IgG, Alexa Fluor 594 goat anti–rabbit IgG, Alexa Fluor 488 goat anti–mouse IgG, and Alexa Fluor 594 goat anti–mouse IgG were from Life Technologies.

Cells and plasmids

BMMs were generated from femurs of C57BL/6J mice and cultured for 6–7 d, as described previously (Knapp and Swanson, 1990). All animal-related procedures were performed in compliance with the University of Michigan guidelines for the humane use of animals. MEFs and HEK293T cells were cultured as described previously (Yoshida et al., 2011). MEFs from TSC2-knockout (Zhang et al., 2003) and WT control mice were provided by D. Kwiatkowski (Harvard Medical School, Boston, MA). The plasmid pIRES-mCFP was constructed by replacing the EGFP sequence of pIRES-EGFP (BD Biosciences) and the PCR-amplified mCFP sequence between BstX1 and Not1. Rac-WT and Rac-N17 sequences were PCR amplified and subcloned into the pIRES-mCFP between Nhe1 and EcoR1 sites, resulting in the plasmids pRac1-WT-IRES2-mCFP and pRac1-N17-IRES2-mCFP, respectively. The plasmid pmCitrine-BtkPH-N1 was described previously (Kamen et al., 2007; Yoshida et al., 2015). In brief, the PCR-amplified BtkPH sequence was subcloned into the pmCitrine-N1 vector (Clontech) between XhoI and HindIII. The plasmid pC 1δ-YFP was a gift from T. Meyer (Stanford University, Palo Alto, CA). The plasmid pEGFP-N1 was from Clontech. The plasmids psPAX2 and pMD2.G were from Addgene. The plasmids pRac1-WT-IRES2-mCFP and pRac1-N17-IRES2-mCFP were derived from pIRES2-EGFP vector (BD Biosciences). The plasmids psPAX2 and pMD2.G were described previously (Suzuki et al., 2013).

Generation of Rac1 knockout MEFs using CRISPR/Cas9 genome editing

The 20-nt guide sequence targeting mouse Rac1 was designed using the CRISPR design tool. The guide RNA (gRNA) encoding DNA was cloned into a bicistronic expression vector (LentiCRISPR v2; a gift from F. Zhang (Broad Institute, Massachusetts Institute of Technology, Cambridge, MA); and plasmid 52961; Addgene) containing human codon–optimized Cas9 and the RNA components (Sanjana et al., 2014). The guiding sequence, with a 3-nt protospacer adjacent motif, targets exon 2 of mouse Rac1 gene: 5′-ACGGTGGGGATGTACTCTCCAGG-3′. As a control, a gRNA sequence targeting GFP was designed (5′-CATGCCTGAAGGTTATGTAC-3′). The LentiCRISPR vectors with different gRNAs were transfected into HEK293T cells with lentiviral packaging plasmid psPAX2 and envelope plasmid pMD2.G. The virus was collected and concentrated as described previously (Suzuki et al., 2013). MEF3 cells (a gift from L. Kotula, Upstate Medical School, Rochester, NY) were used as WT MEFs. 24 h after infection, the cells were selected for resistance to 5 µg/ml puromycin for 48 h. At day 6 after infection, the cells were examined for Rac1 expression and used for further experiments.

Cell treatments

For the biochemical assays, BMMs and MEFs were cultured in DMEM (low glucose; 11885; Life Technologies) without FBS overnight. BMMs were stimulated with M-CSF (6.9 nM) or PMA (100 nM) for the indicated times and lysates were prepared for Western blotting as described previously (Yoshida et al., 2011). For inhibitor treatment assays, BMMs were pretreated with U0126 (10 µM), A66 (3 µM), IC87114 (0.1–1 µM), MK2206 (2 µM), or EIPA (25 µM) for 30 min in DMEM, HBSS, or DPBS containing leucine or glucose. A combination of blebbistatin (75 µM for 35 min) and jasplakinolide (1 µM for 15 min) was also used. After treatments, cells were stimulated by M-CSF or PMA for 5 or 30 min, respectively. For calphostin C treatment, cells were pretreated with 500 nM calphostin C for 20 min in a CO_2 incubator and transferred into a biological safety cabinet for light activation for another 10 min (Bruns et al., 1991). For leucine or glucose stimulation assays, BMMs were treated with DPBS with leucine or glucose at the indicated concentrations for 35 min (for blebbistatin and jasplakinolide experiments) or 50 min and stimulated by M-CSF or PMA for another 5 min or 30 min, respectively. MEFs were starved in DPBS with leucine (0.4 mM) or glucose (5.6 mM) for 30 min and stimulated with PDGF (2 nM) for 15 min (Gao et al., 2007). For inhibitor treatment assays, MEFs were pretreated 30 min with EIPA (25 µM) or the JB combination. For PDGF and leucine stimulation assays, MEFs were incubated in DPBS with glucose (5.6 mM) throughout, including 50 min starvation followed by stimulation for 10 min with PDGF and/or leucine (0.4 mM). For the dipeptide assay, MEFs were cultured in DPBS or DPBS with Ala-Leu (4.0 mM) for 30 min and stimulated by PDGF for another 30 min. For amino acid stimulation assays, BMMs or MEFs were incubated in HBSS (Life Technologies) for 50 min and then DMEM for 5 min with or without M-CSF (BMMs), or 10 min with or without PDGF (MEFs).

Western blotting

Cells were lysed 10 min in ice-cold lysis buffer (40 mM Hepes, pH 7.5, 120 mM NaCl, 1 mM EDTA, 10 mM pyrophosphate, 10 mM glycerophosphate, 50 mM NaF, 1.5 mM Na_3VO_4, 0.3% CHAPS, and a mixture of protease inhibitors; Roche) as reported previously (Yoshida et al., 2011). Lysates were centrifuged at 13,000 *g* for 15 min at 4°C, and the supernatant was mixed with 4× SDS sample buffer and boiled for 5 min. The samples were subjected to SDS-PAGE and applied to Western blotting with the indicated antibodies. At least two independent experiments were performed to confirm the results of pilot studies.

Microscopy

Phase-contrast and fluorescence microscopic images were collected in an Eclipse TE-300 inverted microscope with a 60× NA1.4, oil-immersion PlanApo objective lens (Nikon) and a Lambda LS xenon arc lamp for epifluorescence illumination (Sutter Instruments). Fluorescence excitation and emission wavelengths were selected using a 69008 set (Chroma Technology) and a Lambda 10–2 filter wheel controller (Shutter Instruments) equipped with a shutter for epifluorescence illumination control. Images were recorded with a Photometrics CoolSnap HQ cooled charge-coupled device camera (Roper Scientific).

For live cell imaging, cells plated onto glass-bottom, 35-mm diameter dishes (MatTek Corp.) were preloaded by endocytosis of TRDx (0.5 mg/ml × 2–3 h) followed by a 2- to 4-h chase in unlabeled medium.

Cells were first imaged in Ringer's buffer (RB; 10 mM Hepes, pH 7.2, 155 mM NaCl, 5 mM KCl, 2 mM $CaCl_2$, 1 mM $MgCl_2$, 2 mM NaH_2PO_4, and 10 mM glucose; 23°C), then stimulated with 200 ng/ml M-CSF in RB to stimulate macropinocytosis, with added LY, rinsed, transferred to the microscope, and imaged at 20-s intervals. Images were processed as video or still sequences using MetaMorph software. To confirm the results of live cell imaging, three or more independent experiments were performed.

Immunofluorescence staining for BMMs was performed as described previously (Racoosin and Swanson, 1993). In brief, cells were washed three times with 37°C RB and fixed for 30 min at 37°C with fixation buffer (20 mM Hepes, pH 7.4, 2% PFA, 4.5% sucrose, 70 mM NaCl, 10 mM KCl, 10 mM MgCl2, 2 mM EGTA, 70 mM lysine-HCl, and 10 mM sodium periodate). The fixed cells were rinsed with washing buffer (TBS buffer: 20 mM Tris-HCl, pH 7.4, 150 mm NaCl, 4.5% sucrose) for 3 × 5 min, permeabilized with ice-cold methanol for 20 s and then incubated with blocking buffer (TBS buffer with 2% goat serum) for 30 min at RT. Immunofluorescence staining for MEFs was performed as described previously (Yoshida et al., 2011). The fixed cells were rinsed with DPBS for 3 × 5 min, permeabilized with 0.01% saponin in DPBS for 10 min at RT then blocked with blocking buffer (TBS buffer; 0.01% Triton X-100, and 2% BSA) for 30 min at RT. Samples were incubated with primary antibodies at a dilution of 1:100 in blocking buffer at RT for 2 h. After rinsing three times with TBS buffer, samples were incubated with secondary antibodies at a dilution of 1:200 in blocking buffer at RT for 2 h. After rinsing three times with TBS buffer, samples were mounted on microscope slides using Prolong Gold (Life Technologies). To confirm qualitative observations, quantitative analysis was applied to 10 or more immunofluorescence images.

Macropinosome assay

To measure macropinocytosis, cells on coverslips were pulse labeled for the indicated times with LY (1 mg/ml) or FDx70 (1.2 mg/ml) in medium containing M-CSF, PDGF, or PMA and then were rinsed, fixed, and observed using a Nikon TE300 fluorescence microscope. Uningested probes were removed by gently washing with DPBS before cells were fixed for 30 min at 37°C with fixation buffer. Phase-contrast and FDx70 or LY fluorescence images of fixed cells were captured and merged after reducing background signal using MetaMorph (version 6.3; Molecular Devices). The number of induced macropinosomes per cell was determined by counting FDx70- or LY-positive vesicles on the merged images; >25 cells were observed for each assay.

Quantitative analysis of mTOR-LAMP colocalization

Phase-contrast and mTOR and LAMP-1 immunofluorescence images were taken of BMMs containing tubular endolysosome structures. More than 49 BMM images from five independent experiments were observed per condition, and the frequency of the cells showing mTOR–LAMP-1 was determined by comparing mTOR, LAMP-1, and merge images using MetaMorph. Data were analyzed by the *t* test. To analyze colocalization in MEFs, pilot experiments were followed by one experiment in which >10 MEF images per condition were randomly captured, and LAMP-1 and mTOR images were compared using the "Measure Colocalization" command in MetaMorph, after thresholding each image to reduce background signals. We calculated the area of mTOR-LAMP colocalization divided by the area of LAMP, and the result was considered as the frequency of mTOR–LAMP-1 colocalization in this study. Identical methods were used to quantify colocalization of mTOR with LY. All data were analyzed by the *t* test.

Ratiometric imaging

Cells were prepared for live cell imaging as described by Yoshida et al. (2009). A ratiometric imaging approach was used to measure the ratios of two fluorescent chimeras in BMMs, using MetaMorph software as described previously (Swanson, 2002; Hoppe and Swanson, 2004; Yoshida et al., 2009; Welliver and Swanson, 2012). Ratio images reported the concentrations of YFP-BktPH relative to CFP, to localize PIP_3, and of YFP-C1δ relative to CFP, to localize DAG, thereby correcting for variations in optical path length owing to cell shape. Ratio images of LY and TRDx reported the relative distributions of the two dyes in endocytic compartments. All observations were repeated >10 times.

LY endocytosis

LY was used to investigate the trafficking of small solutes ingested by macropinocytosis. For time course experiments, cells were incubated in DMEM or HBSS with 1 mg/ml LY for 1, 5, or 10 min, with or without M-CSF, and then rinsed three times before fixation. For colocalization assays, cells were stained for immunofluorescence with anti–LAMP or anti–mTOR antibodies. For Rac1 expression experiments, BMMs were transfected with plasmids encoding pRac1-WT-IRES2-mCFP or pRac1-N17-IRES2-mCFP, using a Mouse Macrophage Nucleofector kit (Amaxa). Cells were incubated for 24 h and used for the LY assay. For starvation assays, cells were incubated in HBSS for 30 min before 10-min M-CSF stimulation. To quantify the amount of ingested LY, phase-contrast and LY images were taken and shade/bias corrections were applied (Hoppe, 2007). More than 10 cell images per condition were captured on three separate days, and the total intensity of LY inside each cell was obtained using the "Measure" tool in MetaMorph, after thresholding each image to subtract background signals. To quantify the frequency of mTOR-LY colocalization, phase-contrast, mTOR, and LY images were taken and shade/bias corrections were applied. More than 10 cell images per condition were captured. The frequency of the integrated signal of mTOR (or LY) overlapping of LY (or mTOR) inside of a cell was measured as the frequency of mTOR-LY colocalization using the "Measure Colocalization" tool in MetaMorph. Because we used CFP as a marker for cells overexpressing Rac1 or Rac1(N17), we corrected the LY fluorescence image (I_F: excitation 430/424; emission 535/530) for crossover signal from CFP (I_{CFP}: excitation 430/424; emission 470/424). Crossover fluorescence was corrected by measuring the coefficient β from cells expressing CFP only (I_F/I_{CFP}) and isolating the LY fluorescence from cells containing LY and CFP, using the equation $I_{LY} = I_F - \beta I_{CFP}$ (Hoppe, 2007). All data were analyzed by the *t* test.

Detail of statistical methods

All experimental replicates subsequent to pilot studies are presented here. In scoring for macropinosome formation (Fig. 2, B–F; Fig. 3, A–D and H; Fig. 4, A–G; Fig. 5 B; Fig. 6 I; Fig. S2 C; Fig. S3, C and E; and Fig. S4 F), a one-tailed, paired *t* test was applied to data obtained from three technical replicates of samples with 15 or more cells for each condition. For mTOR-LAMP colocalization analysis in BMMs (Fig. S4 C), a two-tailed, paired *t* test was applied to five technical replicates of samples with seven or more cells for each condition. For analysis of mTOR recruitment to macropinosomes (Fig. S4 G), a one-tailed, paired *t* test was applied to data obtained from three technical replicates of samples with 25 or more macropinosomes for each condition. For mTOR-LAMP colocalization analysis in MEFs (Fig. S5, B, E, and G) and mTOR-LY colocalization analysis in BMMs (Fig. 6, H, K, and M), a one-tailed, two-sample unequal variance *t* test was applied to images of 10 or more cells for each condition. For analysis of integrated intensity of LY in BMMs (Fig. 6, D, J, and L), a one-tailed, two-sample unequal variance *t* test was applied to images of 10 or more cells for each condition.

Online supplemental material

Fig. S1 shows the effects of inhibitors of PI3K, MEK, and Akt on mTORC1 activity in BMMs. Fig. S2 shows PDGF-stimulated macropinocytosis in MEFs. Fig. S3 shows that Rac deficiency abrogates PDGF signaling to mTORC1. Fig. S4 shows mTOR distributions in BMMs relative to internalized LY. Fig. S5 shows amino acid–dependent colocalization of mTOR with LAMP-1 and endocytosed LY in MEFs. Video 1 shows piranhalysis after macropinosome formation in BMMs and corresponds to Fig. 7 A. Video 2 shows the fusion of LY-labeled macropinosomes with TRDx-labeled tubular endolysosomes and corresponds to Fig. 7 B. Video 3 shows the fusion of LY-labeled macropinosomes with TRDx-labeled tubular endolysosomes. Video 4 shows solute size–dependent delivery of dyes from endolysosomes into macropinosomes and corresponds to Fig. 7 C. Video 5 shows solute size–dependent delivery of dyes from endolysosomes into macropinosomes. Online supplemental material is available at http://www.jcb.org/cgi/content/full/jcb.201504097/DC1.

Acknowledgments

The authors thank Lydia Krienke, Samuel Straight, Scott Schreiber, and Brian Gregorka for assistance and Diane Fingar, Adam Hoppe, David Friedman, and Philip King for comments. TSC2-knockout MEFs were generously provided by David Kwiatkowski.

This work was supported by grants from the National Institutes of Health (R01-GM-110215-01 to J.A. Swanson and R01-DK-083491 to K. Inoki) and the University of Michigan Medical School.

The authors declare no competing financial interests.

Submitted: 22 April 2015
Accepted: 2 September 2015

References

Amyere, M., B. Payrastre, U. Krause, P. Van Der Smissen, A. Veithen, and P.J. Courtoy. 2000. Constitutive macropinocytosis in oncogene-transformed fibroblasts depends on sequential permanent activation of phosphoinositide 3-kinase and phospholipase C. *Mol. Biol. Cell.* 11:3453–3467. http://dx.doi.org/10.1091/mbc.11.10.3453

Araki, N., M.T. Johnson, and J.A. Swanson. 1996. A role for phosphoinositide 3-kinase in the completion of macropinocytosis and phagocytosis by macrophages. *J. Cell Biol.* 135:1249–1260. http://dx.doi.org/10.1083/jcb.135.5.1249

Bar-Peled, L., and D.M. Sabatini. 2014. Regulation of mTORC1 by amino acids. *Trends Cell Biol.* 24:400–406. http://dx.doi.org/10.1016/j.tcb.2014.03.003

Bar-Sagi, D., and J.R. Feramisco. 1986. Induction of membrane ruffling and fluid-phase pinocytosis in quiescent fibroblasts by *ras* proteins. *Science.* 233:1061–1068. http://dx.doi.org/10.1126/science.3090687

Berthiaume, E.P., C. Medina, and J.A. Swanson. 1995. Molecular size-fractionation during endocytosis in macrophages. *J. Cell Biol.* 129:989–998. http://dx.doi.org/10.1083/jcb.129.4.989

Blagden, S.P., and A.E. Willis. 2011. The biological and therapeutic relevance of mRNA translation in cancer. *Nat. Rev. Clin. Oncol.* 8:280–291. http://dx.doi.org/10.1038/nrclinonc.2011.16

Bridges, D., K. Fisher, S.N. Zolov, T. Xiong, K. Inoki, L.S. Weisman, and A.R. Saltiel. 2012. Rab5 proteins regulate activation and localization of target of rapamycin complex 1. *J. Biol. Chem.* 287:20913–20921. http://dx.doi.org/10.1074/jbc.M111.334060

Bruns, R.F., F.D. Miller, R.L. Merriman, J.J. Howbert, W.F. Heath, E. Kobayashi, I. Takahashi, T. Tamaoki, and H. Nakano. 1991. Inhibition of protein kinase C by calphostin C is light-dependent. *Biochem. Biophys. Res. Commun.* 176:288–293. http://dx.doi.org/10.1016/0006-291X(91)90922-T

Bubb, M.R., A.M. Senderowicz, E.A. Sausville, K.L. Duncan, and E.D. Korn. 1994. Jasplakinolide, a cytotoxic natural product, induces actin polymerization and competitively inhibits the binding of phalloidin to F-actin. *J. Biol. Chem.* 269:14869–14871.

Chen, J.W., W. Pan, M.P. D'Souza, and J.T. August. 1985. Lysosome-associated membrane proteins: characterization of LAMP-1 of macrophage P388 and mouse embryo 3T3 cultured cells. *Arch. Biochem. Biophys.* 239:574–586.

Chen, C., H.Q. Li, Y.J. Liu, Z.F. Guo, H.J. Wu, X. Li, H.F. Lou, L. Zhu, D. Wang, X.M. Li, et al. 2015. A novel size-based sorting mechanism of pinocytic luminal cargoes in microglia. *J. Neurosci.* 35:2674–2688. http://dx.doi.org/10.1523/JNEUROSCI.4389-14.2015

Commisso, C., S.M. Davidson, R.G. Soydaner-Azeloglu, S.J. Parker, J.J. Kamphorst, S. Hackett, E. Grabocka, M. Nofal, J.A. Drebin, C.B. Thompson, et al. 2013. Macropinocytosis of protein is an amino acid supply route in Ras-transformed cells. *Nature.* 497:633–637. http://dx.doi.org/10.1038/nature12138

Desjardins, M. 1995. Biogenesis of phagolysosomes: the 'kiss and run' hypothesis. *Trends Cell Biol.* 5:183–186. http://dx.doi.org/10.1016/S0962-8924(00)88989-8

Efeyan, A., R. Zoncu, and D.M. Sabatini. 2012. Amino acids and mTORC1: from lysosomes to disease. *Trends Mol. Med.* 18:524–533. http://dx.doi.org/10.1016/j.molmed.2012.05.007

Favata, M.F., K.Y. Horiuchi, E.J. Manos, A.J. Daulerio, D.A. Stradley, W.S. Feeser, D.E. Van Dyk, W.J. Pitts, R.A. Earl, F. Hobbs, et al. 1998. Identification of a novel inhibitor of mitogen-activated protein kinase kinase. *J. Biol. Chem.* 273:18623–18632. http://dx.doi.org/10.1074/jbc.273.29.18623

Feliciano, W.D., S. Yoshida, S.W. Straight, and J.A. Swanson. 2011. Coordination of the Rab5 cycle on macropinosomes. *Traffic.* 12:1911–1922. http://dx.doi.org/10.1111/j.1600-0854.2011.01280.x

Flinn, R.J., Y. Yan, S. Goswami, P.J. Parker, and J.M. Backer. 2010. The late endosome is essential for mTORC1 signaling. *Mol. Biol. Cell.* 21:833–841. http://dx.doi.org/10.1091/mbc.E09-09-0756

Fujii, M., K. Kawai, Y. Egami, and N. Araki. 2013. Dissecting the roles of Rac1 activation and deactivation in macropinocytosis using microscopic photomanipulation. *Sci. Rep.* 3:2385. http://dx.doi.org/10.1038/srep02385

Gao, Y.S., C.C. Hubbert, J. Lu, Y.S. Lee, J.Y. Lee, and T.P. Yao. 2007. Histone deacetylase 6 regulates growth factor-induced actin remodeling and endocytosis. *Mol. Cell. Biol.* 27:8637–8647. http://dx.doi.org/10.1128/MCB.00393-07

Hirai, H., H. Sootome, Y. Nakatsuru, K. Miyama, S. Taguchi, K. Tsujioka, Y. Ueno, H. Hatch, P.K. Majumder, B.S. Pan, and H. Kotani. 2010. MK-2206, an allosteric Akt inhibitor, enhances antitumor efficacy by standard chemotherapeutic agents or molecular targeted drugs in vitro and in vivo. *Mol. Cancer Ther.* 9:1956–1967. http://dx.doi.org/10.1158/1535-7163.MCT-09-1012

Hoppe, A.D. 2007. Quantitative FRET microscopy of live cells. *In* Imaging Cellular and Molecular Biological Functions. S.L. Shorte, and F. Frischknecht, editors. Springer, New York. 157–181. http://dx.doi.org/10.1007/978-3-540-71331-9_6

Hoppe, A.D., and J.A. Swanson. 2004. Cdc42, Rac1, and Rac2 display distinct patterns of activation during phagocytosis. *Mol. Biol. Cell.* 15:3509–3519. http://dx.doi.org/10.1091/mbc.E03-11-0847

Huotari, J., and A. Helenius. 2011. Endosome maturation. *EMBO J.* 30:3481–3500. http://dx.doi.org/10.1038/emboj.2011.286

Inoki, K., Y. Li, T. Zhu, J. Wu, and K.L. Guan. 2002. TSC2 is phosphorylated and inhibited by Akt and suppresses mTOR signalling. *Nat. Cell Biol.* 4:648–657. http://dx.doi.org/10.1038/ncb839

Jamieson, S., J.U. Flanagan, S. Kolekar, C. Buchanan, J.D. Kendall, W.J. Lee, G.W. Rewcastle, W.A. Denny, R. Singh, J. Dickson, et al. 2011. A drug targeting only p110α can block phosphoinositide 3-kinase signalling and tumour growth in certain cell types. *Biochem. J.* 438:53–62. http://dx.doi.org/10.1042/BJ20110502

Jewell, J.L., R.C. Russell, and K.L. Guan. 2013. Amino acid signalling upstream of mTOR. *Nat. Rev. Mol. Cell Biol.* 14:133–139. http://dx.doi.org/10.1038/nrm3522

Jewell, J.L., Y.C. Kim, R.C. Russell, F.X. Yu, H.W. Park, S.W. Plouffe, V.S. Tagliabracci, and K.L. Guan. 2015. Differential regulation of mTORC1 by leucine and glutamine. *Science.* 347:194–198. http://dx.doi.org/10.1126/science.1259472

Kamen, L.A., J. Levinsohn, and J.A. Swanson. 2007. Differential association of phosphatidylinositol 3-kinase, SHIP-1, and PTEN with forming phagosomes. *Mol. Biol. Cell.* 18:2463–2472. http://dx.doi.org/10.1091/mbc.E07-01-0061

Knapp, P.E., and J.A. Swanson. 1990. Plasticity of the tubular lysosomal compartment in macrophages. *J. Cell Sci.* 95:433–439.

Koivusalo, M., C. Welch, H. Hayashi, C.C. Scott, M. Kim, T. Alexander, N. Touret, K.M. Hahn, and S. Grinstein. 2010. Amiloride inhibits macropinocytosis by lowering submembranous pH and preventing Rac1 and Cdc42 signaling. *J. Cell Biol.* 188:547–563. http://dx.doi.org/10.1083/jcb.200908086

Li, L., E. Kim, H. Yuan, K. Inoki, P. Goraksha-Hicks, R.L. Schiesher, T.P. Neufeld, and K.L. Guan. 2010. Regulation of mTORC1 by the Rab and Arf GTPases. *J. Biol. Chem.* 285:19705–19709. http://dx.doi.org/10.1074/jbc.C110.102483

Loewith, R., E. Jacinto, S. Wullschleger, A. Lorberg, J.L. Crespo, D. Bonenfant, W. Oppliger, P. Jenoe, and M.N. Hall. 2002. Two TOR complexes, only one of which is rapamycin sensitive, have distinct roles in cell growth control. *Mol. Cell.* 10:457–468. http://dx.doi.org/10.1016/S1097-2765(02)00636-6

Menon, S., C.C. Dibble, G. Talbott, G. Hoxhaj, A.J. Valvezan, H. Takahashi, L.C. Cantley, and B.D. Manning. 2014. Spatial control of the TSC complex integrates insulin and nutrient regulation of mTORC1 at the lysosome. *Cell.* 156:771–785. http://dx.doi.org/10.1016/j.cell.2013.11.049

Mercer, J., M. Schelhaas, and A. Helenius. 2010. Virus entry by endocytosis. *Annu. Rev. Biochem.* 79:803–833. http://dx.doi.org/10.1146/annurev-biochem-060208-104626

Palm, W., Y. Park, K. Wright, N.N. Pavlova, D.A. Tuveson, and C.B. Thompson. 2015. The utilization of extracellular proteins as nutrients is suppressed by mTORC1. *Cell.* 162:259–270. http://dx.doi.org/10.1016/j.cell.2015.06.017

Porat-Shliom, N., Y. Kloog, and J.G. Donaldson. 2008. A unique platform for H-Ras signaling involving clathrin-independent endocytosis. *Mol. Biol. Cell.* 19:765–775. http://dx.doi.org/10.1091/mbc.E07-08-0841

Racoosin, E.L., and J.A. Swanson. 1989. Macrophage colony-stimulating factor (rM-CSF) stimulates pinocytosis in bone marrow-derived macrophages. *J. Exp. Med.* 170:1635–1648. http://dx.doi.org/10.1084/jem.170.5.1635

Racoosin, E.L., and J.A. Swanson. 1993. Macropinosome maturation and fusion with tubular lysosomes in macrophages. *J. Cell Biol.* 121:1011–1020. http://dx.doi.org/10.1083/jcb.121.5.1011

Rebsamen, M., L. Pochini, T. Stasyk, M.E. de Araújo, M. Galluccio, R.K. Kandasamy, B. Snijder, A. Fauster, E.L. Rudashevskaya, M. Bruckner, et al. 2015. SLC38A9 is a component of the lysosomal amino acid sensing machinery that controls mTORC1. *Nature.* 519:477–481. http://dx.doi.org/10.1038/nature14107

Ridley, A.J., H.F. Paterson, C.L. Johnston, D. Diekmann, and A. Hall. 1992. The small GTP-binding protein rac regulates growth factor-induced membrane ruffling. *Cell.* 70:401–410. http://dx.doi.org/10.1016/0092-8674(92)90164-8

Roux, P.P., B.A. Ballif, R. Anjum, S.P. Gygi, and J. Blenis. 2004. Tumor-promoting phorbol esters and activated Ras inactivate the tuberous sclerosis tumor suppressor complex via p90 ribosomal S6 kinase. *Proc. Natl. Acad. Sci. USA.* 101:13489–13494. http://dx.doi.org/10.1073/pnas.0405659101

Saci, A., L.C. Cantley, and C.L. Carpenter. 2011. Rac1 regulates the activity of mTORC1 and mTORC2 and controls cellular size. *Mol. Cell.* 42:50–61. http://dx.doi.org/10.1016/j.molcel.2011.03.017

Sancak, Y., T.R. Peterson, Y.D. Shaul, R.A. Lindquist, C.C. Thoreen, L. Bar-Peled, and D.M. Sabatini. 2008. The Rag GTPases bind raptor and mediate amino acid signaling to mTORC1. *Science.* 320:1496–1501. http://dx.doi.org/10.1126/science.1157535

Sanjana, N.E., O. Shalem, and F. Zhang. 2014. Improved vectors and genome-wide libraries for CRISPR screening. *Nat. Methods.* 11:783–784. http://dx.doi.org/10.1038/nmeth.3047

Shaw, R.J., and L.C. Cantley. 2006. Ras, PI(3)K and mTOR signalling controls tumour cell growth. *Nature.* 441:424–430. http://dx.doi.org/10.1038/nature04869

Straight, A.F., A. Cheung, J. Limouze, I. Chen, N.J. Westwood, J.R. Sellers, and T.J. Mitchison. 2003. Dissecting temporal and spatial control of cytokinesis with a myosin II Inhibitor. *Science.* 299:1743–1747. http://dx.doi.org/10.1126/science.1081412

Suzuki, T., D. Bridges, D. Nakada, G. Skiniotis, S.J. Morrison, J.D. Lin, A.R. Saltiel, and K. Inoki. 2013. Inhibition of AMPK catabolic action by GSK3. *Mol. Cell.* 50:407–419. http://dx.doi.org/10.1016/j.molcel.2013.03.022

Swanson, J.A. 1989. Phorbol esters stimulate macropinocytosis and solute flow through macrophages. *J. Cell Sci.* 94:135–142.

Swanson, J.A. 2002. Ratiometric fluorescence microscopy. *In* Molecular Cellular Biology. Vol. 31. P. Sansonetti, and A. Zychlinsky, editors. Academic Press, New York. 1–18.

Swanson, J.A. 2008. Shaping cups into phagosomes and macropinosomes. *Nat. Rev. Mol. Cell Biol.* 9:639–649. http://dx.doi.org/10.1038/nrm2447

Swanson, J.A., and C. Watts. 1995. Macropinocytosis. *Trends Cell Biol.* 5:424–428. http://dx.doi.org/10.1016/S0962-8924(00)89101-1

Tee, A.R., R. Anjum, and J. Blenis. 2003. Inactivation of the tuberous sclerosis complex-1 and -2 gene products occurs by phosphoinositide 3-kinase/Akt-dependent and -independent phosphorylation of tuberin. *J. Biol. Chem.* 278:37288–37296. http://dx.doi.org/10.1074/jbc.M303257200

Veithen, A., P. Cupers, P. Baudhuin, and P.J. Courtoy. 1996. v-Src induces constitutive macropinocytosis in rat fibroblasts. *J. Cell Sci.* 109:2005–2012.

Wang, S., Z.Y. Tsun, R.L. Wolfson, K. Shen, G.A. Wyant, M.E. Plovanich, E.D. Yuan, T.D. Jones, L. Chantranupong, W. Comb, et al. 2015. Lysosomal amino acid transporter SLC38A9 signals arginine sufficiency to mTORC1. *Science.* 347:188–194. http://dx.doi.org/10.1126/science.1257132

Welliver, T.P., and J.A. Swanson. 2012. A growth factor signaling cascade confined to circular ruffles in macrophages. *Biol. Open.* 1:754–760. http://dx.doi.org/10.1242/bio.20121784

Welliver, T.P., S.L. Chang, J.J. Linderman, and J.A. Swanson. 2011. Ruffles limit diffusion in the plasma membrane during macropinosome formation. *J. Cell Sci.* 124:4106–4114. http://dx.doi.org/10.1242/jcs.091538

Willingham, M.C., and S.S. Yamada. 1978. A mechanism for the destruction of pinosomes in cultured fibroblasts. Piranhalysis. *J. Cell Biol.* 78:480–487. http://dx.doi.org/10.1083/jcb.78.2.480

Yoshida, S., A.D. Hoppe, N. Araki, and J.A. Swanson. 2009. Sequential signaling in plasma-membrane domains during macropinosome formation in macrophages. *J. Cell Sci.* 122:3250–3261. http://dx.doi.org/10.1242/jcs.053207

Yoshida, S., S. Hong, T. Suzuki, S. Nada, A.M. Mannan, J. Wang, M. Okada, K.L. Guan, and K. Inoki. 2011. Redox regulates mammalian target of rapamycin complex 1 (mTORC1) activity by modulating the TSC1/TSC2-Rheb GTPase pathway. *J. Biol. Chem.* 286:32651–32660. http://dx.doi.org/10.1074/jbc.M111.238014

Yoshida, S., I. Gaeta, R. Pacitto, L. Krienke, O. Alge, B. Gregorka, and J.A. Swanson. 2015. Differential signaling during macropinocytosis in response to M-CSF and PMA in macrophages. *Front. Physiol.* 6:8. http://dx.doi.org/10.3389/fphys.2015.00008

Zhang, H., G. Cicchetti, H. Onda, H.B. Koon, K. Asrican, N. Bajraszewski, F. Vazquez, C.L. Carpenter, and D.J. Kwiatkowski. 2003. Loss of Tsc1/Tsc2 activates mTOR and disrupts PI3K-Akt signaling through downregulation of PDGFR. *J. Clin. Invest.* 112:1223–1233. http://dx.doi.org/10.1172/JCI200317222

Zoncu, R., L. Bar-Peled, A. Efeyan, S. Wang, Y. Sancak, and D.M. Sabatini. 2011a. mTORC1 senses lysosomal amino acids through an inside-out mechanism that requires the vacuolar H(+)-ATPase. *Science.* 334:678–683. http://dx.doi.org/10.1126/science.1207056

Zoncu, R., A. Efeyan, and D.M. Sabatini. 2011b. mTOR: from growth signal integration to cancer, diabetes and ageing. *Nat. Rev. Mol. Cell Biol.* 12:21–35. http://dx.doi.org/10.1038/nrm3025